

Bone tissue microwave tomography: Is there any information of micro-structure?

R.M.Irastorza^a, C. M. Carlevaro^{a,b}, F. Vericat^a

^a*Instituto de Física de Líquidos y Sistemas Biológicos (IFLYSIB-CCT La Plata-CONICET), Calle 59 No 789, B1900BTE La Plata, Argentina.*

^b*Universidad Tecnológica Nacional - FRBA, UDB Física, Mozart No 2300, C1407IVT Buenos Aires, Argentina.*

Abstract

In this work two dimensional simulations of ellipses models and realistic models of trabecular bone microstructure tissue are performed. The results presented here intend to show that microstructure is an important factor in the effective dielectric properties of trabecular bone. The main idea is to analyze the possibility of using the dielectric behaviour of bone tissue as a measurement of bone health. The frequency used was 950MHz. It was found that dielectric properties can be used as a estimate of degree of anisotropy, particularly, conductivity shown better results. For representing bone tissue effective models were also tested. Ellipses models with aspect ratio $a/b = 1.5$ shown relative good agreement. As a final conclusion according to the results presented here, anisotropy must be taken into account when measuring trabecular bone tissue with microwave imaging.

Keywords: FDTD, bone dielectric properties, microwave tomography.

1. Introduction

Osteoporosis is usually diagnosed by one parameter: bone mineral density (BMD). Unfortunately, it does not give direct tissue biomechanical information. There is a continuous search of several alternative methods for *in vivo* estimation of bone mechanical properties. In this regard, ultrasound seems to be the most advanced tool[1]. Other approaches, like that developed by Kanis and co-workers [2], intend to integrate the risks associated with clinical risk factors and BMD at the femoral neck.

Measurement of dielectric properties of bones has been recently received some

attention due to its potential application as an alternative diagnostic method for evaluating bone health [3, 4, 5, 6, 7, 8]. Low frequency *in vitro* measurements on a particular sample (human cadavers, age = 58 ± 20 years) have shown that linear combination of two relative permittivities in frequency ranges (50Hz-1kHz and 100kHz-5MHz), is able to predict 73% of the trabecular bone volume fraction (ratio of bone volume to total tissue volume BV/TV) [9]. Clearly, at the state of the art, low frequency methods are only applicable to special cases of open surgery. Recently, the first relative permittivity and conductivity *in vivo* bone images have been obtained by microwave tomography [10, 11]. Furthermore, *in vitro* microwave studies suggest a negative correlation between bone mineral density and permittivity / conductivity [12, 13]. This agrees with the results of reference [14]. There, it is hypothesized that mineralized bones have lower relative permittivity mainly due to a lower water content.

It is well known that not only mineral content but also microstructure defines the mechanical and dielectric properties of bone tissue [9]. There exist several parameters to characterize microstructure of bone, among others: BV / TV, mean intercept length (MIL), trabecular thickness[15]. In reference [3] a theoretical approach for porosity estimation is developed. The authors use effective dielectric properties to obtain the spectral function of the bone, which is close related with its porosity.

Age and pathological conditions produce selective bone tissue resorption [16] (pag 326), which results in thinner horizontal trabeculae. Efforts have done in order to detect this anisotropy by using ultrasound techniques [17, 18]. In those papers, the author uses fast and slow waves, which can propagate in the direction of the major trabecular orientation. Regarding this, trabecular bone was found to be electrically anisotropic. The relationships between the dielectric properties at low frequency ($< 10\text{MHz}$) in different directions have been early studied by Saha et. al [19]. These variations could be interpreted by trabecular orientation, but there is no strong evidence about it yet. However, at low frequency ($< 10\text{MHz}$), no linear correlation between degree of anisotropy and dielectric or electrical parameters was found by Sierpowska et al. [9].

In electromagnetic simulation and theory of hierarchical materials, homogenization techniques are extensively used [20]. They give information of microstructure [21] and anisotropy [22]. This paper intend to give a step toward a microstructure modeling of trabecular bone tissue. We study effective dielectric approaches and their application to realistic electromagnetic models

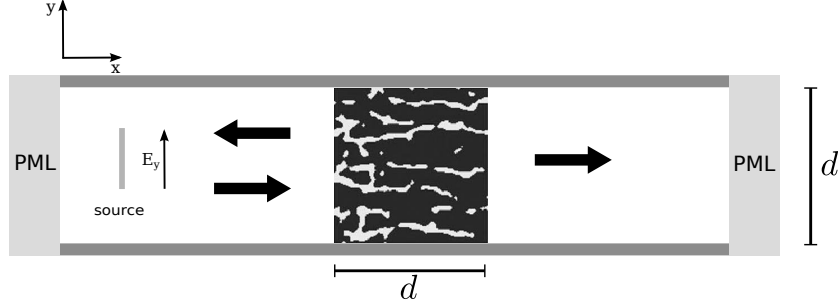


Figure 1: Simulation box.

based on scanning electron microscopy images of bone tissue. The main idea is to study the anisotropy of trabecular microstructure and its relationships with the dielectric effective parameters using simulation techniques. The two dimensional (2D) models used here are numerically solved by finite difference time domain (FDTD) [23, 24]. We will try to answer one important question: If we are interested in measuring trabecular bone at microwave range, is it confident to consider isotropic effective dielectric properties? At the same time, the answer can contribute to the development of a tool for microstructure characterization of bone tissue by effective models which take account anisotropy.

2. Methods

Effective relative permittivity (ϵ_{eff}) calculus in 2D is study by observing the reflection of a slice of relative dielectric constant ϵ_e with inclusions of relative permittivity ϵ_i . Figure 1 shows the simulation box. Two shapes of inclusion are tested: circular and elliptical. For validation purposes, different values of ϵ_e (σ_e) and ϵ_i (σ_i) are tested (where σ_x is the conductivity of medium x). In all the cases overlapping is allowed. For simulation of realistic models of trabecular bone, we will also consider it as two phase material: the trabeculae as inclusions and bone marrow as background. Values of permittivity and conductivity are obtained from [25], which is based on [26].

2.1. Numerical models

Maxwell equations are numerically solved using finite difference time domain (FDTD)[24]. The implementation of FDTD algorithm is performed

using *meep*[23]. The slice is a square with variable thickness (d). The entire simulation box has variable length and it is adjusted large enough in order to reach three times the thickness of the sample at each side. A temporal gaussian pulse polarized in y direction (E_y) with central frequency equal to 950MHz is used as source, located far enough from the interface air-slice. The resolution of the simulation box is $350\mu\text{m}$ (or smaller) and the Courant number is $S = 0.5$. In x direction boundary condition is a perfectly matched load (PML).

In order to obtain the ε_{eff} the reflection coefficient of the medium with inclusions or bone ($\Gamma_i(\omega)$) is compared to an homogeneous block $\Gamma(\omega, \varepsilon_{\text{eff}})$ in the frequency range of interest. Minimization of the absolute difference ($|\Gamma_i(\omega) - \Gamma(\omega, \varepsilon_{\text{eff}})|$) is performed using a Newton conjugate-gradient algorithm (implemented in Scipy 0.9.0 [27]).

Scripts *ad hoc* in Python 2.7.2 [28] were developed to process the simulation data. In order to study different number of inclusions and also randomly locate circles and ellipses, *ad hoc* python routines were used as well.

2.2. Effective permittivity models

There are several models which represent effective dielectric properties of two-phase materials, Appendix A shows some of them. In these models, effective values depend on the fraction occupied by the inclusions (ϕ_i) and on the permittivities (conductivities) ε_e (σ_e) and ε_i (σ_i). They also depend on shape and anisotropy. Those models which take into account shape and anisotropy are of particular interest for this work [22], specifically elliptical inclusions will be studied here. The general form used for Mejdoubi and Brusseau [22] is:

$$\varepsilon_{\text{eff}} = \varepsilon_e \cdot f\left(\frac{\varepsilon_i}{\varepsilon_e}, \phi_i, A\right) \approx \varepsilon_e (1 + \alpha\phi_i + \beta\phi_i^2) \quad (1)$$

where α and β depend on depolarization factor (A) and are detailed in Appendix A. For instance, one approximation of these parameters are: $\alpha = 1/[A + 1/(\varepsilon_i/\varepsilon_e - 1)]$ and β can take two values, we will use:

$$\beta_{\text{SBG}} = \frac{\frac{\varepsilon_i}{\varepsilon_e}}{A^2 \left(\frac{\varepsilon_i}{\varepsilon_e} - 1\right) \left(1 + \frac{1}{A \left(\frac{\varepsilon_i}{\varepsilon_e} - 1\right)}\right)^3} \quad (2)$$

the other approximation can be found in the Appendix A. From now on we call this model as M-B. The depolarization factor intrinsically has the information of shape and orientation of inclusions. For instance, for elliptical inclusions with 90° of orientation respect to the applied electric field, aspect ratio (semimajor axis a / semiminor axis b) $a/b = 1/3$ and $\varepsilon_i/\varepsilon_e = 20/2$, Mejdoubi and Brusseau obtained A equal to 0.732 or 0.772, using β_{MG} or β_{SBG} , as defined in Appendix A, respectively. It is remarkable that these values were fitted with $\phi_i < 0.1$.

2.3. Micro-structure Parameters

Trabecular bone structure has been extensively studied and there are several parameters to characterize it (see for instance [15]). In this work four parameters are studied from 2D images of trabecular bones: BV / TB, trabecular thickness, mean intercept length (MIL) and degree of anisotropy ($DA = MIL_{max}/MIL_{min}$). The former is associated with bone porosity and the latter with anisotropy. For BV / TB and MIL calculus, see [15] and references therein. For the trabecular thickness calculus we trace n parallel lines in ortogonal direction with respect to the main trabecular direction (we define it as angle $\eta(MIL_{max})$), measuring the thickness of the intersections with trabeculae.

2.4. Images

Images used here are available in [29] and in reference [17]. These images are used to build the realistic dielectric models and image processing is applied in order to define the two-phase material[30].

Samples used here are named as sample 1, 2, 3, 4, 5 and 6, they are all shown in section 3 (Fig.6). Figure 2 shows just some of them. Figure 2 (a) shows trabecular bone tissue from an old person (sample 1), its porosity is approximately 0.75. Polar plot in Fig.2 (d) shows the corresponding MIL parameter (η is the slope angle of the parallel lines for MIL calculus). It seems to be isotropic, the maximum of the MIL parameter is around 0° but it almost a circle. Figure 2 (b) shows a highly porous old bone as well with porosity equal to 0.79 (sample 2). Clearly its MIL maximumm is around 90° (see Fig.2 (e)). Figure 2 (c) shows a young bone (sample 3) with porosity equal to 0.46 and 0° main direction (Fig.2 (f)).

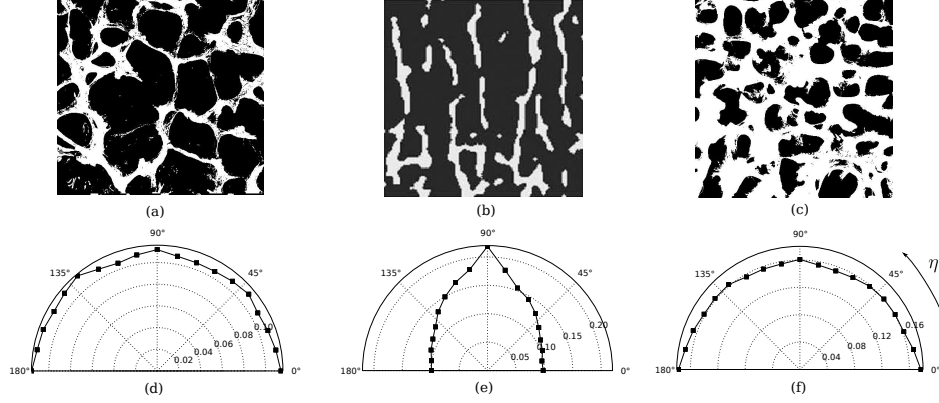


Figure 2: Microscopic characterization of main direction: mean intercept length calculus. (a), (b) and (c) correspond to sample 1, 2 and 3 as defined in the text (see subsection 2.4), respectively. (d), (e) and (f) are the polar plots of the MIL parameter and correspond to sample 1, 2 and 3, respectively. η is the slope angle of the parallel lines for MIL calculus. The lines are guides for the eyes.

3. Results

3.1. Validation

Validation of method is performed using an hexagonal array of discs, it has an analytic solution [31] (see Fig.3). Figures 3 (a) and (b) correspond to inclusions of air embedded in a matrix with $\varepsilon_e = 16$ and $\sigma_e = 0.043$ S/m. Figures 3 (c) and (d) correspond to a potential model of trabecular bone tissue. Inclusions are the trabeculae and the matrix is the bone marrow. These validation media were also used by Bonifasi-Lista and Charkaeve [4]. Values are $\varepsilon_e = 5.485$ (bone marrow), $\varepsilon_i = 20.584$ (trabeculae) and $\sigma_e = 0.043$ S/m (bone marrow), $\sigma_i = 0.364$ S/m (trabeculae). The fraction occupied is varied by changing the disc radius. A good agreement is observed.

Disc shape inclusions randomly located are also tested (see Fig.4 (a)) with similar values to those used in reference [21]. An excellent agreement is observed. Different circle radii are tested, it can be seen that permittivity and conductivity do not depend on the radius but on the fraction occupied (ϕ_i). It is known that not only fraction occupied by the inclusions determines the effective dielectric properties but also their shape[22]. Ellipse shape inclusion media are tested with effective formulae obtained by reference [22] (see Appendix A). The only difference to Mejdoubi and Brosseau work is that, here, orientation of the ellipses is a random angle with normal distribution

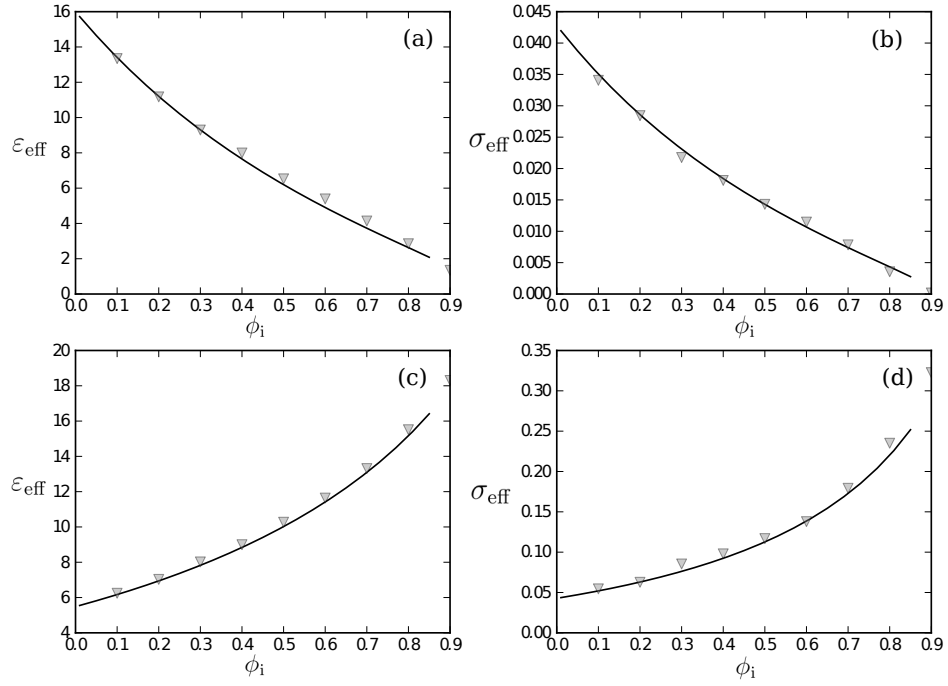


Figure 3: Effective permittivity and conductivity of hexagonal array discs as a function of fraction occupied (ϕ_i). Comparison between analytic solution (continuous line) and simulation (∇). (a) and (b) correspond to the effective permittivity and conductivity of a medium with $\epsilon_i, \epsilon_e = 1.0, 16.0$ and $\sigma_i, \sigma_e = 0.0, 0.043$. (c) and (d) correspond to the effective permittivity and conductivity of a medium with $\epsilon_i, \epsilon_e = 20.584, 5.485$ and $\sigma_i, \sigma_e = 0.364, 0.043$

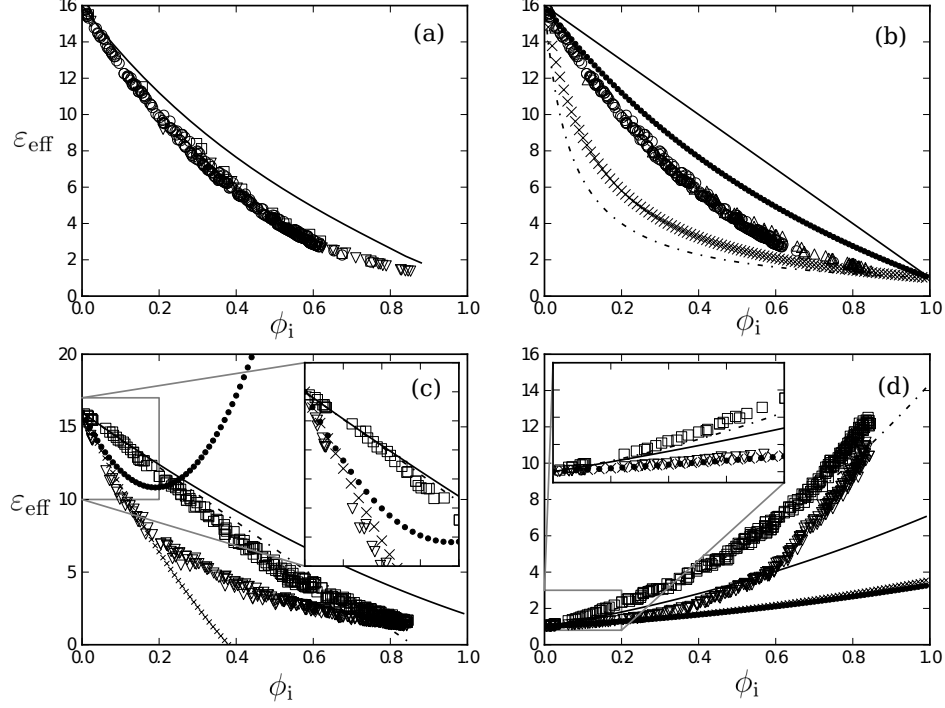


Figure 4: Effective relative permittivity of media with disc and ellipse shape inclusions randomly located. (a) Medium with discs for different radius (r_1 , r_2 and r_3 , ∇ , \square and \circ , respectively) compared with analytic solution of hexagonal array (continuous line). $r_1 < r_2 < r_3$. (b) Effective permittivity of discs (\circ) compared to ellipses at $\hat{\gamma} = 45^\circ$ (Δ) and Wiener (continuous and dash-dotted lines) and H-S (cross and dotted lines) bounds. (c)-(d) Effective permittivity of oriented ellipses at $\hat{\gamma} = 0^\circ$ (∇), 90° (\square) compared to M-B bounds (dotted and continuous marks for β_{MG} , cross and dashed-dotted marks for β_{SBG}). In (a), (b) and (c) $\varepsilon_i, \varepsilon_e = 1, 16$. In (d) $\varepsilon_i, \varepsilon_e = 16, 1$.

($\gamma \sim N(\hat{\gamma}, \sigma^2 = 100)$). Three mean values of orientation are evaluated $\hat{\gamma} = 0^\circ, 45^\circ$ and 90° . For all mentioned above cases overlapping of inclusions is allowed. Figure 4 (b) shows comparison between ellipses ($\hat{\gamma} = 45^\circ$) with discs and effective bounds (Eqs.A.1-A.4). In Figures 4 (c) and (d) comparison between ellipse shape inclusion media and bounds (Eq.1) is shown. Even these models were fitted for $\phi_i < 0.1$, a relative good agreement is observed for fraction occupied < 0.2 if β_{SBG} formula is used (see dashed-dot and cross marked in Figs.4 (c) and (d)).

Figure 5 (a) shows an example of a model totally anisotropic. Ellipses are oriented and arranged in parallel lines. The slope of the lines is varied an

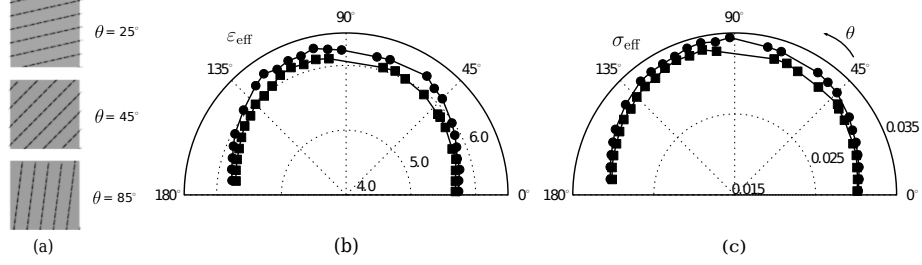


Figure 5: Ellipse models. Percolated (\circ) and not percolated (\square) models. The lines are guides for the eyes. (a) Simulation slice examples. (b)-(c) Polar plots for effective relative permittivity and effective conductivity, respectively. θ is the slope angle of the oriented ellipses which is coincident with the slope of the lines (see text for explanation).

angle θ (see Fig.5 (a)) and the effective dielectric properties are calculated. Source is always y polarized, named E_y , and $\phi_i \approx 0.054$. Two kind of models are tested, allowing (percolated) and not (not percolated) overlapping of ellipses. Note that, at the simulation frequency of this work (950MHz), percolated and not percolated systems have a similar behaviour. M-B model using β_{SBG} gives depolarization factor $A = 0.901$ for $E_y \perp MIL_{\text{max}}$ and $A = 0.120$ for $E_y \parallel MIL_{\text{max}}$, which gives $\varepsilon_{\text{eff}} = 5.729, 6.120$ and $\sigma_{\text{eff}} = 0.046, 0.054$ S/m, respectively. Values obtained by numerical simulations are $\varepsilon_{\text{eff}} = 5.689, 6.120$ and $\sigma_{\text{eff}} = 0.045, 0.053$ S/m. We see that the agreement between simulations and effective models is relatively good.

3.2. Simulation of realistic models

Figure 6 shows the samples used here to build the realistic models. Models are simulated as a two phase medium where trabeculae are the inclusions and the background is the bone marrow. The images are rotated an angle θ (at 30 degree steps) and the simulation is performed (the same method, as explained in subsection 2.1, is used to calculate the effective dielectric properties). The applied field is always y polarized.

Table 1 resumes their micro-structure parameters (calculated as described in subsection 2.3). There is only a young sample (sample 3). Sample 1 and 3 have the lower DA values.

Table 2 shows the dielectric properties of samples we have obtained. θ_{max} y θ_{min} are the angles for which dielectric properties are maximum ($\varepsilon_{\text{eff}_{\text{max}}}$ and $\sigma_{\text{eff}_{\text{max}}}$) and minimum ($\varepsilon_{\text{eff}_{\text{min}}}$ and $\sigma_{\text{eff}_{\text{min}}}$), respectively. It is remarkable that ε_{eff} and σ_{eff} are maxima when the applied field is totally aligned with the main direction of the sample ($\eta(MIL_{\text{max}})$). In this table the ratios $\varepsilon_{\text{eff}_{\text{max}}}/\varepsilon_{\text{eff}_{\text{min}}}$ and

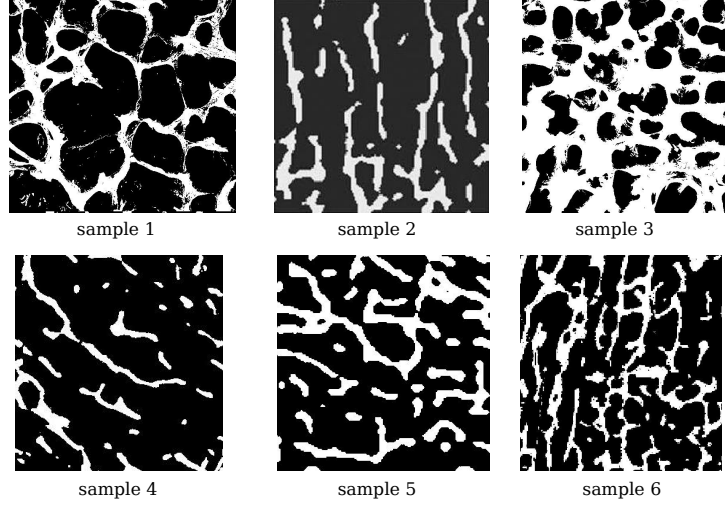


Figure 6: Samples.

Table 1: Microstructure properties.

Sample	Porosity	BV/TV	$\eta(\text{MIL}_{\max})$	Trab. Thick. [mm] $\pm\text{std}$	DA
1	0.75	0.25	0°	0.11 ± 0.16	1.08
2	0.79	0.21	90°	0.18 ± 0.13	2.23
3	0.46	0.54	0°	0.23 ± 0.32	1.14
4	0.88	0.12	130°	0.13 ± 0.08	1.53
5	0.74	0.26	90°	0.21 ± 0.19	1.40
6	0.74	0.26	90°	0.13 ± 0.14	1.42

Table 2: Effective dielectric properties obtained by simulation of realistic models.

Sample	θ_{\max}	θ_{\min}	$\varepsilon_{\text{eff}_{\max}}$	$\varepsilon_{\text{eff}_{\min}}$	$\frac{\varepsilon_{\text{eff}_{\max}}}{\varepsilon_{\text{eff}_{\min}}}$	$\sigma_{\text{eff}_{\max}}$	$\sigma_{\text{eff}_{\min}}$	$\frac{\sigma_{\text{eff}_{\max}}}{\sigma_{\text{eff}_{\min}}}$
1	90°	30°	7.503	7.096	1.06	0.077	0.0706	1.09
2	0°	90°	6.950	6.247	1.12	0.069	0.054	1.28
3	90°	0°	11.446	10.345	1.11	0.154	0.149	1.18
4	120°	30°	6.119	5.864	1.04	0.053	0.048	1.10
5	0°	60°	7.312	6.798	1.07	0.075	0.063	1.19
6	0°	90°	7.189	6.782	1.06	0.071	0.063	1.13

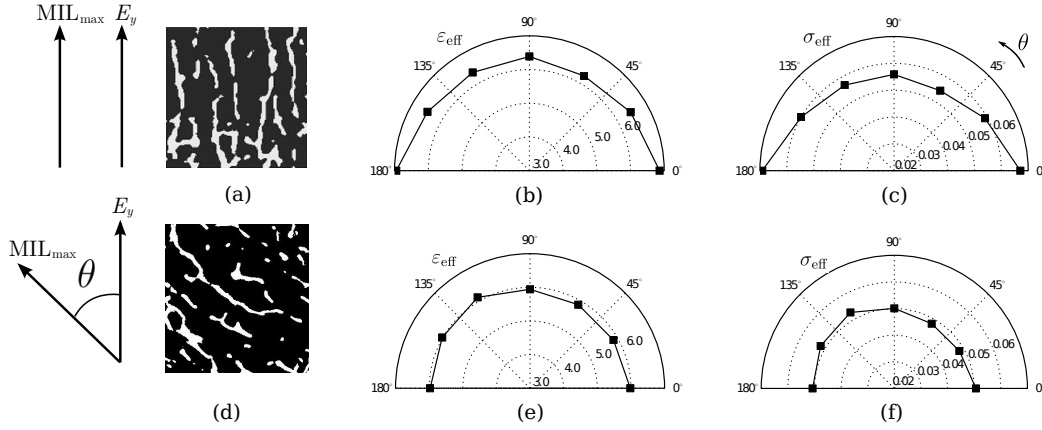


Figure 7: Effective dielectric properties of sample 2 (a-c) and sample 4 (d-f) as a function of angle (θ). (a) and (d) show the samples and main direction. (b) and (e) effective relative permittivity. (c) and (f) effective conductivity. The lines are guides for the eyes.

$\sigma_{\text{eff}_{\max}}/\sigma_{\text{eff}_{\min}}$ are also shown. It is observed that the latter always gives larger values than the former. See for instance: sample 2, it has the maximum degree of anisotropy (2.23) and the maximum of conductivity ratio (1.28) as well, while permittivity ratio is 1.12. Figure 7 shows typical simulations of sample 2 (Fig.7 (a)) and 4 (Fig.7 (b)). Polar plots shows effective relative permittivity and conductivity as a function of θ . (b) and (c) correspond to sample 2 and (e) and (f) correspond to sample 4. It should be noted that main direction can be detected by both permittivity and conductivity.

3.3. Effective models

In this subsection comparison between effective models and realistic models are performed. It was shown in [22] that depolarization factor (a scalar

Table 3: Effective M-B models using β_{SBG} .

a/b		$\phi_i \equiv BV/TV$				
		0.12	0.21	0.25	0.26	0.54
1.0	ε_{eff}	6.688	7.103	7.342	7.565	10.703
	σ_{eff}	0.065	0.066	0.071	0.073	0.124
1.5	$\frac{\varepsilon_{\text{eff}_{\text{max}}}}{\varepsilon_{\text{eff}_{\text{min}}}}$	$\frac{6.471}{6.245} \approx \mathbf{1.04}$	$\frac{7.342}{6.910} \approx \mathbf{1.06}$	-	$\frac{7.873}{7.315} \approx \mathbf{1.07}$	-
	$\frac{\sigma_{\text{eff}_{\text{max}}}}{\sigma_{\text{eff}_{\text{min}}}}$	$\frac{0.057}{0.053} \approx \mathbf{1.09}$	$\frac{0.071}{0.062} \approx \mathbf{1.14}$	-	$\frac{0.080}{0.068} \approx \mathbf{1.19}$	-
	$\frac{\varepsilon_{\text{eff}_{\text{max}}}}{\varepsilon_{\text{eff}_{\text{min}}}}$	$\frac{6.744}{6.129} \approx 1.10$	$\frac{7.844}{6.689} \approx 1.17$	-	$\frac{8.512}{7.028} \approx 1.21$	-
	$\frac{\sigma_{\text{eff}_{\text{max}}}}{\sigma_{\text{eff}_{\text{min}}}}$	$\frac{0.064}{0.051} \approx 1.25$	$\frac{0.085}{0.058} \approx 1.47$	-	$\frac{0.098}{0.062} \approx 1.58$	-

in 2D) for media with elliptical inclusions depends on aspect ratio (a/b) and orientation. As it is shown in Fig.4 effective M-B models have relative good agreement for $\phi_i < 0.2$ when β_{SBG} is used. In general this result was observed for several simulations not shown here. Table 3 shows some results of M-B models (using β_{SBG}) as a function of ϕ_i . We replace ϕ_i by BV/TV parameter of each sample. Three aspect ratios are observed: $\frac{a}{b} = 1.0, 1.5$ and 3.0 . Note that, for high values of DA, although the absolute values agree relatively, the correlation with the relative values of $\frac{a}{b} = 1.5$ is even better (values highlighted in boldface).

4. Discussion

Results in this paper are limited to a central frequency (950MHz). This choice was based on the fact that most of the works on microwave tomography use this frequency. Moreover, practical implementation are generally developed in frequency domain, based on network analyzer plus antenna array. Therefore we assume that constant values of permittivity and conductivity of each component of bone tissue (trabecular and bone marrow) are a good representation of a real measurement.

Recent works have begun to study microwave imaging of bone tissue *in vitro* [10, 12] and *in vivo* [11]. In general, the current interest is to find correlations between dielectric properties and bone mineral density or bone volume. It is surprising that the relationship between anisotropy and dielectric properties has been relatively little studied. We will mainly focus this discussion into two aspects: firstly, we will present the correlation between BV/TV and

effective dielectric properties and, secondly, we will comment the results on anisotropy.

Comparison between dielectric properties and bone volume of Table 1 and 2 shows a positive relationship. This means, the higher BV/TV the higher effective permittivity and conductivity. This is very intuitive and is in accordance with two phase models: when the fraction of inclusion (with higher relative permittivity) grows so do the permittivity and conductivity. Differences are found when this simulation results are compared to measurements *in vivo*. In reference [11] the authors found that an affected calcaneus (with a lower bone volume) has a 23% higher relative permittivity as compared to a normal one. It is necessary to remark that it is just one sample without statics support. The same group has recently published a paper on *in vitro* measurements of trabecular porcine femur samples (six bone specimens in saline solution)[12]. They studied variation of dielectric properties as a function of mineralization. Degree of mineralization was altered (not naturally) by acid treatment, their results are in agreement with their previous work [11]. It also agrees with [13], in which degree of mineralization was measured and negative correlation between bone mineral density and relative permittivity was found (six samples of human osteoporotic trabecular samples in saline solution, it is also a small number of samples).

Some simple calculation can be performed with the help of effective models. For instance, using Eq.1 for a total aligned electric field and bone orientation with $\phi_i = 0.26$, $\varepsilon_i = 20.584$, $\sigma_i = 0.364$ and $\varepsilon_e = 78.00$, $\sigma_e = 1.39$ (similar values to 0.9% saline solution) gives 61.76 and 1.08, for permittivity and conductivity, respectively. For $\phi_i = 0.54$ gives 42.79 and 0.749. These results give a possible explanation of the relation between BV/TS and dielectric effective properties (at least for *in vitro* measurements): samples with lower BV/TV have more space for water or saline solution, which increases their permittivity and conductivity. Special care must be taken for interpreting *in vivo* measurements. What is taken the place of bone in a resorption process: Is it predominantly some high water content connective tissue/cells/blood (high dielectric properties) or is it bone marrow (low dielectric properties)? As first image *in vivo* has shown[11], it seems that a loss of bone tissue increases both permittivity and conductivity, then first option could be the more feasible process.

Regarding anisotropy, Table 2 shows that polarized electric field totally aligned with main direction of the sample gives the higher relative permittivity and conductivity. On the contrary, minimum values are found if the

electric field and main direction are ortogonal.

Table 2 also shows that degree of anisotropy correlates relatively well with permittivity ratio ($\varepsilon_{\text{eff}_{\text{max}}}/\varepsilon_{\text{eff}_{\text{min}}}$). Maximum value of DA (2.23) for sample 2 gives also maximum ratio of relative permittivity (1.12). In this case, permittivity is 12% higher when the electric field is totally aligned with the main direction. Conductivity ratio (righth most column of Table 2) shows the strongest relationship with DA, in the case mentioned before conductivity is 28% higher when there is a total alignment. As a concluding remark of these results: conductivity could be a better estimate of DA.

Effective ellipses models are more approximated when fraction occupied is low, strictly speaking for $\phi_i < 0.1$. Table 3 resumes the application to trabecular bone tissue. It can be seen a relative good agreement for $BV/TV < 0.26$ (see Table 3 values in boldface). For instance, sample 2, 4, 5 and 6 have similar values to those given for a ellipses model with aspect ratio $a/b = 1.5$. It shows an interesting trend: ellipse models represent well samples with high degree of anisotropy and low fraction occupied. On the other hand, when samples have low DA and low fraction occupied circular inclusions models seem to be better.

As a final conclusion, we can say that samples with high degree of anisotropy can give until 20% of difference between aligned and ortogonal conductivity values. Relative permittivity shows lower variation. Semenov et al. [10] studied microwave-tomographic imaging of the high dielectric-contrast objects (as bone tissue and muscle or skin). Several difficulties of reconstruction algorithms were found by the authors even by taking bone as isotropic tissue. Microwave imaging of bone tissue is still in its begining, but according to the results presented here, anisotropy must be taken into account when measuring trabecular bone tissue.

Acknowledgements

This work was supported by grants from the National Council for Scientific and Technical Research (CONICET) of Argentina.

Appendix A. Effective approaches

Wiener approach (W)

$$\varepsilon_{\text{eff}_{\text{max}}} = \phi_i \varepsilon_i + (1 - \phi_i) \varepsilon_e \quad (\text{A.1})$$

$$\varepsilon_{\text{eff}_{\min}} = \frac{\varepsilon_i \varepsilon_e}{(1 - \phi_i) \varepsilon_i + \phi_i \varepsilon_e} \quad (\text{A.2})$$

Hashin-Strikman approach (H-S)

$$\varepsilon_{\text{eff}_{\max}} = \varepsilon_e + \frac{\phi_i}{\frac{1}{\varepsilon_i - \varepsilon_e} + \frac{1 - \phi_i}{2\varepsilon_e}} \quad (\text{A.3})$$

$$\varepsilon_{\text{eff}_{\min}} = \varepsilon_i + \frac{1 - \phi_i}{\frac{1}{\varepsilon_e - \varepsilon_i} + \frac{\phi_i}{2\varepsilon_i}} \quad (\text{A.4})$$

Mejdoubi-Brosseau approach (M-B)

$$\varepsilon_{\text{eff}} = \varepsilon_e \cdot f\left(\frac{\varepsilon_i}{\varepsilon_e}, \phi_i, A\right) \approx \varepsilon_e (1 + \alpha \phi_i + \beta \phi_i^2) \quad (\text{A.5})$$

with $\alpha = 1/[A + 1/(\varepsilon_i/\varepsilon_e - 1)]$ and β can take two values depending on the approach:

$$\beta_{\text{MG}} = \frac{1}{A + \frac{2}{\frac{\varepsilon_i}{\varepsilon_e} - 1} + \frac{1}{A} \left(\frac{1}{\frac{\varepsilon_i}{\varepsilon_e} - 1} \right)^2}$$

or

$$\beta_{\text{SBG}} = \frac{\frac{\varepsilon_i}{\varepsilon_e}}{A^2 \left(\frac{\varepsilon_i}{\varepsilon_e} - 1 \right) \left(1 + \frac{1}{A \left(\frac{\varepsilon_i}{\varepsilon_e} - 1 \right)} \right)^3}.$$

References

- [1] M. Haidekker, G. Dougherty, Medical Imaging in the Diagnosis of Osteoporosis and Estimation of the Individual Bone Fracture Risk, Springer, 2011.
- [2] J. Kanis, W. H. O. C. for Metabolic Bone Diseases, Assessment of osteoporosis at the primary health care level, WHO Collaborating Centre for Metabolic Bone Diseases, University of Sheffield Medical School, 2008.

- [3] E. Cherkaev, C. Bonifasi-Lista, Characterization of structure and properties of bone by spectral measure method, *Journal of Biomechanics* 44 (2) (2011) 345–351.
- [4] C. Bonifasi-Lista, E. Cherkaev, Electrical impedance spectroscopy as a potential tool for recovering bone porosity, *Physics in medicine and biology* 54 (2009) 3063.
- [5] J. Sierpowska, M. Lammi, M. Hakulinen, J. Jurvelin, R. Lappalainen, J. Toyraas, Effect of human trabecular bone composition on its electrical properties, *Medical engineering & physics* 29 (8) (2007) 845–852.
- [6] J. Sierpowska, Electrical and Dielectric Characterization of Trabecular Bone Quality, University of Kuopio, 2007.
- [7] J. Sierpowska, M. Hakulinen, J. Töyräs, J. Day, H. Weinans, J. Jurvelin, R. Lappalainen, Prediction of mechanical properties of human trabecular bone by electrical measurements, *Physiological measurement* 26 (2005) S119.
- [8] J. Sierpowska, J. Töyräs, M. Hakulinen, S. Saarakkala, J. Jurvelin, R. Lappalainen, Electrical and dielectric properties of bovine trabecular bone relationships with mechanical properties and mineral density, *Physics in medicine and biology* 48 (2003) 775.
- [9] J. Sierpowska, M. Hakulinen, J. Töyräs, J. Day, H. Weinans, I. Kiviranta, J. Jurvelin, R. Lappalainen, Interrelationships between electrical properties and microstructure of human trabecular bone, *Physics in medicine and biology* 51 (2006) 5289.
- [10] S. Semenov, A. Bulyshev, A. Abubakar, V. Posukh, Y. Sizov, A. Souvorov, P. van den Berg, T. Williams, Microwave-tomographic imaging of the high dielectric-contrast objects using different image-reconstruction approaches, *Microwave Theory and Techniques, IEEE Transactions on* 53 (7) (2005) 2284–2294.
- [11] A. Golnabi, P. Meaney, S. Geimer, T. Zhou, K. Paulsen, Microwave tomography for bone imaging, in: *Biomedical Imaging: From Nano to Macro*, 2011 IEEE International Symposium on, IEEE, 2011, pp. 956–959.

- [12] P. Meaney, T. Zhou, D. Goodwin, A. Golnabi, E. Attardo, K. Paulsen, Bone dielectric property variation as a function of mineralization at microwave frequencies, *International Journal of Biomedical Imaging* 2012.
- [13] R. M. Irastorza, Identificación de sistemas: aplicación a la evaluación in vitro de la calidad ósea en tejido trabecular humano, Ph.D. thesis, National University of La Plata, Argentina. (Sep. 2010).
URL <http://sedici.unlp.edu.ar/?id=ARG-UNLP-TPG-0000001486>
- [14] A. Peyman, Dielectric properties of tissues; variation with age and their relevance in exposure of children to electromagnetic fields; state of knowledge, *Progress in Biophysics and Molecular Biology*.
- [15] A. Odgaard, *Bone Mechanics*, CRC Press LLC, 2001.
- [16] E. Orwoll, *Osteoporosis in Men*, Wiley Online Library, 1999.
- [17] A. Hosokawa, Numerical analysis of variability in ultrasound propagation properties induced by trabecular microstructure in cancellous bone, *Ultrasonics, Ferroelectrics and Frequency Control*, IEEE Transactions on 56 (4) (2009) 738–747.
- [18] A. Hosokawa, Effect of porosity distribution in the propagation direction on ultrasound waves through cancellous bone, *Ultrasonics, Ferroelectrics and Frequency Control*, IEEE Transactions on 57 (6) (2010) 1320–1328.
- [19] S. Saha, P. Williams, Comparison of the electrical and dielectric behavior of wet human cortical and cancellous bone tissue from the distal tibia, *Journal of orthopaedic research* 13 (4) (1995) 524–532.
- [20] F. Teixeira, Time-domain finite-difference and finite-element methods for maxwell equations in complex media, *Antennas and Propagation*, IEEE Transactions on 56 (8) (2008) 2150–2166.
- [21] K. Kärkkäinen, A. H. Sihvola, K. I. Nikoskinen, Effective permittivity of mixtures: numerical validation by the fdtd method, *IEEE Transactions on Geoscience and Remote Sensing* 38 (3) (2000) 1303–1308.
- [22] A. Mejdoubi, C. Brosseau, Finite-element simulation of the depolarization factor of arbitrarily shaped inclusions, *Physical Review E* 74 (3) (2006) 031405.

- [23] A. Oskooi, D. Roundy, M. Ibanescu, P. Bermel, J. Joannopoulos, S. Johnson, Meep: A flexible free-software package for electromagnetic simulations by the fdtd method, *Computer Physics Communications* 181 (3) (2010) 687–702.
- [24] A. Hagness, S. Taflove, *Computational electrodynamics: The finite-difference time-domain method*, 3rd Edition, Artech House, Inc., 2005.
- [25] Dielectric properties of body tissues.
URL <http://niremf.ifac.cnr.it/tissprop>
- [26] S. Gabriel, R. Lau, C. Gabriel, The dielectric properties of biological tissues: Iii. parametric models for the dielectric spectrum of tissues, *Physics in medicine and biology* 41 (1996) 2271.
- [27] Scientific tools for python.
URL <http://www.scipy.org/>
- [28] Python programming language.
URL <http://www.python.org/>
- [29] Paul hansma research group.
URL <http://hansmalab.physics.ucsb.edu>
- [30] Scikits-image, image processing in python.
URL <http://scikits-image.org/>
- [31] W. T. Perrins, D. R. McKenzie, R. C. McPhedran, Transport properties regular of arrays of cylinder, *Proc. R. Soc. Lond. A* 369 (1979) 207–225.